J Electr Eng Technol.2017; 13(?): 1921-718
http://doi.org/10.???/JEET.2017.13.1.1921

ISSN(Print) 1975-0102
ISSN(Online) 2093-7423

Ultrasonic Distance Measurement Method by Using the Envelope Model of Received Signal Based on System Dynamic Model of Ultrasonic Transducers

Jin-Hee Choe*, Kook-Sun Lee, Ick Choy*** and Whang Cho†**

Abstract – In order to acquire an accurate *TOF* , this paper proposes a method that produces *TOF* by using a mathematical model for the envelope of the received signal obtained from a system dynamic model of ultrasonic transducer. The proposed method estimates the arrival time of the received signal retrospectively by comparing its wave form obtained after triggering point with its mathematical envelope model. Experimental result shows that the error due to variation of triggering point can be dramatically decreased by implementing the proposed method.

Keywords: Envelope model, Least square algorithm, System dynamic model of ultrasonic transducer, Time of flight, Ultrasonic distance measurement

1. Introduction

An accurate measurement of distance using time of flight (*TOF*) of ultrasonic wave is fundamental to a wide variety of engineering applications. For example, distance measurement in robotics is useful in localization, map building, object tracking, obstacle avoidance, and camera lens focusing [1-5].

In these applications, ultrasonic distance measurement systems have various advantages over other techniques such as camera based techniques, radio frequency techniques like GPS [6], optical techniques (e.g., laser scanner). This is because ultrasonic techniques may be implemented in such a way that is typically inexpensive, light in weight, and compact in size.

Currently, however, the *TOF* is usually obtained by using simple window comparator which is very unreliable because triggering point is not consistent but varied as much as a multiple of the period of the ultrasonic wave used as the amplitude of the received wave is altered. For frequently used 40 kHz ultrasonic wave, the triggering time can be changed as a multiple of 25us which corresponds to the fluctuation in distance measurement by multiples of about 8.5mm.

Two major approaches used to overcome this problem are cross-correlation methods and retrospective estimation methods. In cross-correlation method [7-9], a template signal and received signal are cross-correlated and the time at which the cross-correlation attains the maximum is used as an estimation of *TOF* . Disadvantages of this method come from the fact that in order to increase the estimation accuracy fast sampling rate is required, implying more data, and therefore the required computation burden is squarely proportionally raised. Furthermore, when the shape of received signal is fairly deformed relative to the template signal due to noise or sampling delay, the maximum point may not be consistent.

In retrospective estimation methods of *TOF* [10-13], some mathematical models for the envelope of received signal are developed to fit the data of the received signal and *TOF* is obtained by estimating the arrival time of the received signal retrospectively based on the fitted envelope model. These methods are relatively simple, but very error prone because the mathematical model for the envelope of received signal is simplified so much that it is barely able to model the very beginning part of the received signal, whose information is often very easy to be deteriorated due to noise and triggering delay.

In this paper, a more robust and accurate retrospective estimation method is proposed. Here, a more sophisticated model for the envelope of received signal is developed based on the system dynamic model of piezoelectric system used in typical ultrasonic transducers.

This paper is organized as follows. In Section 2 a complete system dynamic model of piezoelectric transmitter and receiver is developed and used to find the received signal model in response to transmitted signal. In Section 3, a method for ultrasonic distance measurement is proposed based on the envelope model of received signal. Section 4 presents some experimental results and finally some conclusions are derived in Section 5.

2. Ultrasonic Transducer Model

The constitutive relationship of a typical piezoelectric

† Corresponding Author: School of Robotics, Kwangwoon University, Korea.(robot@ kw.ac.kr)
* School of Robotics, Kwangwoon University, Korea. (sokgkgk@ hanmail.net)
** Department of Electrical and Information Engineering, SNUT, Korea. (ksl1222@gmail.com)
*** School of Robotics, Kwangwoon University, Korea. (ickchoy@ kw.ac.kr)
Received: January 20, 2016; Accepted: November 4, 2017

element used in ultrasonic transducer is given by [14]

$$\begin{pmatrix} q \\ x \end{pmatrix} = \begin{pmatrix} C & p \\ p & 1/k \end{pmatrix} \begin{pmatrix} v \\ f \end{pmatrix} \tag{1}$$

where constants and variables are defined as follows.

q : electric charge [C]
x : displacement [m]
v : applied voltage [V]
f : applied force [N]
C : capacitance when $f = 0$ [F]
k : stiffness or spring constant when $v = 0$ [N/m]
p : piezoelectric constant [C/N or m/V]

The wave generated from ultrasonic transmitter is propagated to ultrasonic receiver through air medium. Assuming the wave is plane wave, the pressure developed at air may be expressed as [15]

$$p_s(x,t) = -\rho c^2 \frac{\partial u(x,t)}{\partial x} = \rho c \dot{u}(x,t) \tag{2}$$

where variables and constants are defined as

p_s : sound pressure [N/m^2 or Pa]
u : particle displacement [m]
. $\dot{u}$: particle velocity [m/s]
ρ : volumetric mass density [kg/m^3]
c : speed of sound [m/s]

2.1 Ultrasonic transmitter model

Fig. 1 shows a schematic diagram for piezoelectric transducer with attached mass, which is used as an ultrasonic sound transmitter. The subscript 't' attached to parameters indicates that the corresponding parameters are defined for the ultrasonic sound transmitter.

The force f_t, developed by the voltage v_t applied at piezoelectric transducer is obtained from Eqn. (1) as

$$f_t = k_t x_t - k_t p_t v_t \tag{3}$$

From Eqn. (2), the reaction force F_t from medium at transmitter face can be expressed as

$$F_t = S_t \rho c \dot{x}_t \tag{4}$$

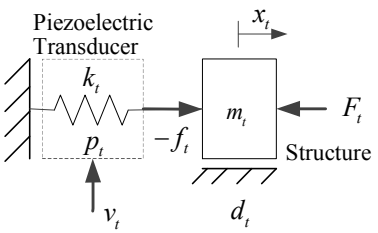

Fig. 1. Ultrasonic transmitter model

where S_t denotes the effective area of transmitter face.

From Newton's law applied to the system shown in Fig. 1, the equation of motion can be obtained as

$$m_t \ddot{x}_t + \left(d_t + S_t \rho c\right)\dot{x}_t + k_t x_t = k_t p_t v_t \tag{5}$$

Eqn. (5) yields the transfer function between the applied voltage v_t and the displacement of transducer x_t as

$$\frac{X_t(s)}{V_t(s)} = \frac{A_t}{s^2 + 2\sigma_t s + \omega_{nt}^2} = \frac{A_t}{\left(s + \sigma_t\right)^2 + \omega_{dt}^2} \tag{6}$$

where

$\omega_{nt} = \sqrt{k_t / m_t}$, $\sigma_t = \varsigma_t \omega_{nt} = \left(d_t + S_t \rho c\right)/2m_t$,

$\omega_{dt} = \sqrt{1-\varsigma_t^2}\,\omega_{nt}$, and $A_t = \dfrac{k_t p_t}{m_t}$.

For a typical ultrasonic transducer, the damping coefficient ς takes value between 0.02 and 0.2. In this case, the following statement can be made for model simplification.

$$\zeta \ll 1 \;\Rightarrow\; \omega_d \approx \omega_n,\ \frac{\sigma}{\omega_d} \ll 1 \tag{7}$$

If input voltage is sinusoidal as $v_t(t) = V_{mt} \sin \omega t$, Eqn. (6) may be rewritten as

$$\frac{X_t(s)}{A_t V_{mt}} = \frac{1}{\left(s + \sigma_t\right)^2 + \omega_{dt}^2} \frac{\omega}{s^2 + \omega^2} \tag{8}$$

From Eqn. (8), the time response of the system can be produced as

$$\begin{aligned} \frac{x_t(t)}{A_t V_{mt}} = {} & K_1 e^{-\sigma_t t} \cos \omega_{dt} t + \frac{K_2}{\omega_{dt}} e^{-\sigma_t t} \sin \omega_{dt} t \\ & + K_3 \cos \omega t + \frac{K_4}{\omega} \sin \omega t \end{aligned} \tag{9}$$

where

$$\begin{aligned} K_1 &= -K_3 = \frac{2\sigma_t \omega}{\left(\omega_{nt}^2 - \omega^2\right)^2 + 4\sigma_t^2 \omega^2} \\ K_2 &= \frac{\omega\left\{2\sigma_t^2 - \left(\omega_{nt}^2 - \omega^2\right)\right\}}{\left(\omega_{nt}^2 - \omega^2\right)^2 + 4\sigma^2 \omega^2} \\ K_4 &= \frac{\omega\left(\omega_{nt}^2 - \omega^2\right)}{\left(\omega_{nt}^2 - \omega^2\right)^2 + 4\sigma_t^2 \omega^2} \end{aligned} \tag{10}$$

When $\omega = \omega_{dt}$, the condition given in Eqn. (7) can be applied to Eqn. (9) and (10) to yield

$$x_t(t) \approx -X_{mt}\left(1-e^{-\sigma_t t}\right)\cos\omega_{dt}t \tag{11}$$

where $X_{mt} = \dfrac{A_t V_{mt}}{2\sigma_t \omega_{dt}}$.

Notice that Eqn. (11) shows that the envelope of $x_t(t)$ is very closely approximated by the unit step response of the following 1st order system.

$$G(s) = X_{mt}\frac{\sigma_t}{s+\sigma_t} \tag{12}$$

The force at transmitter face can be obtained using Eqns. (4), (7), and (11) as

$$F_t(t) \approx F_{mt}\left(1-e^{-\sigma_t t}\right)\sin\omega_{dt}t \tag{13}$$

where $F_{mt} = S_t \rho c \omega_{dt} X_{mt}$.

2.2 Ultrasonic receiver model

Fig. 2 depicts a schematic diagram for piezoelectric transducer with attached mass, which is used as an ultrasonic sound receiver. The subscript 'r' attached to parameters indicates that the corresponding parameters are defined for the ultrasonic sound receiver.

The force created at the face of transmitter is propagated through air with some attenuation, and arrives at the face of the receiver after some delay measured by TOF. Hence, the force applied to the face of the receiver can be expressed as

$$F_r(t') = \alpha F_t(t') - S_r \rho c \dot{x}_r \tag{14}$$

where $t' = t - TOF$, α is the amplitude attenuation factor, and S_r is the effective area of receiver face.

Assuming the charge stored in the piezoelectric element at the receiver is completely discharged to zero, i.e., $q_r = 0$ when the ultrasonic wave is arrived, the induced force f_r and the resulting voltage v_r can be obtained from Eqn. (1) as

$$f_r = k_r^{'} x_r \tag{15}$$

$$v_r = -\frac{p_r}{C_r} f_r = -\frac{p_r}{C_r} k_r^{'} x_r \tag{16}$$

where $k_r^{'} = C_r k_r / (C_r - p_r^2 k_r)$.

Hence, the mathematical model for the system given in Fig. 2 may be expressed as

$$m_r \ddot{x}_r + \left(d_r + S_r \rho c\right)\dot{x}_r + k_r^{'} x_r = \alpha F_t \tag{17}$$

From Eqn. (17), the transfer function between the applied force F_t and the displacement of transducer x_r

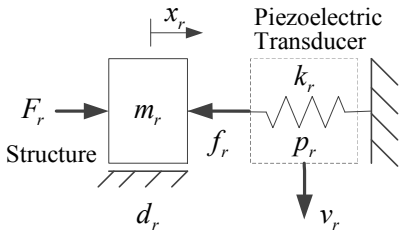

Fig. 2. Ultrasonic receiver model

may be expressed as

$$\frac{X_r(s)}{F_t(s)} = \frac{A_r}{s^2 + 2\sigma_r s + \omega_{nr}^2} = \frac{A_r}{\left(s+\sigma_r\right)^2 + \omega_{dr}^2} \tag{18}$$

where

$\omega_{nr} = \sqrt{k_r^{'}/m_r}$, $\sigma_r = \zeta\omega_{nr} = \left(d_r + S_r\rho c\right)/2m_r$,

$\omega_{dr} = \sqrt{1-\zeta_r^2}\,\omega_{nr}$, and $A_r = \alpha/m_r$.

As is often the case, it can be assumed that the system characteristics of ultrasonic transmitter and receiver are the same so that $\omega_{dt} = \omega_{dr} = \omega_d$, $\sigma_t = \sigma_r = \sigma$. Then, Eqns. (13) and (18) yield

$$\frac{X_r(s)}{A_r F_{mt}} = X_{r1}(s) - X_{r2}(s) \tag{19}$$

where

$$X_{r1}(s) = \frac{1}{\left(s+\sigma\right)^2 + \omega_d^2}\frac{\omega_d}{s^2+\omega_d^2} \tag{20}$$

$$X_{r2}(s) = \frac{\omega_d}{\left\{\left(s+\sigma\right)^2 + \omega_d^2\right\}^2} \tag{21}$$

Eqs. (20) and (21) can be inverse transformed to result in

$$\frac{x_{r1}(t')}{A_r F_{mt}} \approx -\frac{1}{2\sigma\omega_d}\left(1-e^{-\sigma t'}\right)\cos\omega_d t' \tag{22}$$

$$\frac{x_{r2}(t')}{A_r F_{mt}} = \frac{1}{2\omega_d^2} e^{-\sigma t'}\left(\sin\omega_d t' - \omega_d t' \cos\omega_d t'\right) \tag{23}$$

Applying the condition given in Eqn. (7), the final response of $x_r(t')$ can be approximated by

$$\begin{aligned} x_r(t') &= x_{r1}(t') - x_{r2}(t') \\ &\approx -X_{mr}\left\{1-\left(1+\sigma t'\right)e^{-\sigma t'}\right\}\cos\omega_d t' \end{aligned} \tag{24}$$

where $X_{mr} = A_r F_{mt}/2\sigma\omega_d$.

Notice that Eqn. (24) shows that the envelope of $x_r(t')$ corresponds to the unit step response of the following 2nd order system.

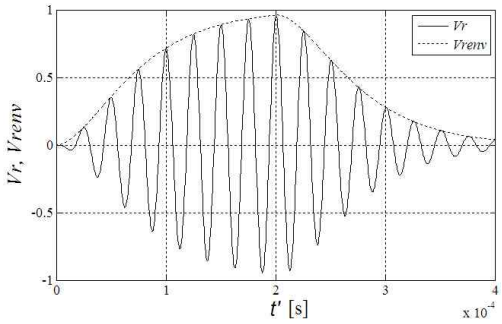

Fig. 3. Simulation for v_r and v_{renv} (pattern 1)

$$G(s) = X_{mr}\frac{\sigma^2}{(s+\sigma)^2} \tag{25}$$

The envelope of the output voltage from receiver, $v_{renv}(t)$, can be obtained from Eqn. (16) and (24).

$$v_{renv}(t) = V_{mr}\left[1-\{1+\sigma(t-TOF)\}e^{-\sigma(t-TOF)}\right]\cdot u(t-TOF) \tag{26}$$

where $V_{mr} = X_{mr}p_r k_r^{'}/C_r$ and $u(t)$ is the unit step function.

Fig. 3 shows the simulation result of v_r and v_{renv} for the case of applying 8 periods of sinusoidal input voltage with circular frequency $\omega_d = 2\pi\cdot 40\times 10^3$ rad/s. Here, damping ratio $\varsigma = 0.1$ is used and the result is normalized by V_{mr}. The figure indicates that when the condition given in Eqn. (7) is satisfied, v_{renv} given in Eqn. (26) coincides very closely with the envelope of v_r.

3. Proposed Method for Distance Measurement

In order to acquire TOF, this paper proposes a method that first collects ADC sampled data of the received signal right after being triggered by some preset threshold voltage, and then estimates the TOF by fitting the data in least square sense to the Eqn. (26). Details are given below.

Step 1: Reset receiver timer to zero at the moment when voltage is applied to the transmitter. The synchronization between transmitter and receiver is accomplished by RF communication.

Step 2: Received signal is appropriately amplified and then compared with preset threshold voltage. At the moment when the received signal firstly rises above the threshold voltage, the time is marked as t_{trig} and ADC sampling is started. The time stamp of the sampled data is calculated by using t_{trig} and ADC sampling rate.

Step 3: After removing DC offset from the sampled data and normalizing the resulting data with its maximum, the following second order low pass filter is used to filter out possible measurement noise.

$$G_{LPF}(s) = \frac{2\omega_d^2}{(s+\omega_d)^2} \tag{27}$$

The filter given in Eqn. (27) is designed so that the gain and phase lag at ω_d are one and $\pi/2$ radian, respectively, and is implemented digitally. To remove the data corresponding transient phase of the filter, the first one or two periods of data are neglected.

Step 4: After taking absolute values of the filtered v_r, peaks values, v_{rpks}, and corresponding time stamp values, t_{rpks}, are sought. Then, t_{rpks} values are compensated in view of the inevitable phase lag caused by filtering process in step 3 above.

Step 5: The data obtained in Step 4 is fitted to Eqn. (26) in least square sense using Levenberg-Marquardt method [16]. In the fitting process, not only TOF but also σ and normalized V_{mr} are used as fitting parameters as well.

For convenience sake, square wave is used instead of sinusoidal wave as input voltage pattern. In this case, in addition to the fundamental wave of amplitude $4V_{mt}/\pi$, higher odd nth harmonics with amplitude $4V_{mt}/n\pi$ may be generated but their effect may be neglected because their frequency are far from the resonance frequency of the transmitter.

In order to increase the fitting accuracy, input voltage patterns are generated such that the envelope of the received signal contains large changes in magnitude and thereby shows some characteristic features. Here, it should be noted that the length of signal pattern should be short enough to avoid the corruption of the received signal, especially at trailing part, by reflected wave. In this paper two patterns are used and results are compared.

Pattern 1: As shown in Fig. 3, eight periods (T) of square wave is applied. The envelope equation is

$$v_{renv,1}(t) = v_{renv}(t) - v_{renv}(t-8T) \tag{28}$$

Pattern 2: Eight periods of square wave is generated and then is followed by additional eight periods of square wave with phase reversed. The envelope equation is

$$v_{renv,2}(t) = v_{renv}(t) - 2v_{renv}(t-8T) + v_{renv}(t-16T) \tag{29}$$

Fig. 4 shows simulation result of applying pattern 2. The result is depicted by normalizing v_r and v_{renv} and shows

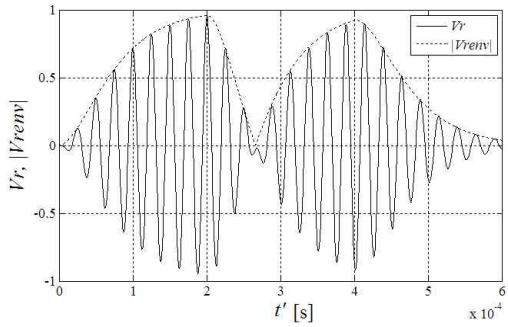

Fig. 4. Simulation for v_r and v_{renv} (pattern 2)

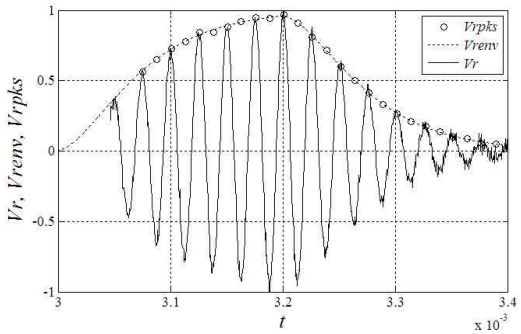

Fig. 5. v_r , v_{rpks} , v_{renv} (pattern 1)

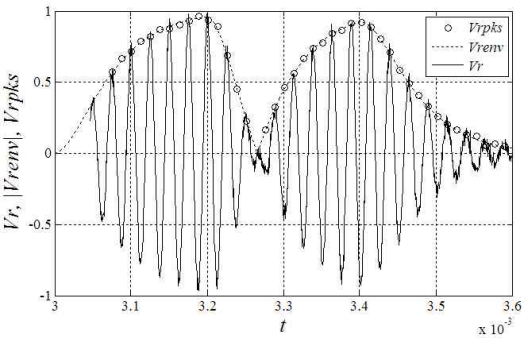

Fig. 6. v_r , v_{rpks} , v_{renv} (pattern 2)

that the approximated v_{renv} matches very closely with the envelope of v_r . As shown in Fig. 4, pattern 2 signal generates two envelope bumps of v_{renv} . This feature will be shown to help to increase the accuracy of TOF measurement in comparison to the case of using pattern 1 signal.

In order to validate the proposed method by simulation, system parameters are chosen as $\omega_d = 2\pi \cdot 40 \times 10^3$ rad/s , $\varsigma = 0.1$, $TOF = 3$ [ms] , $t_{trig} = 3.047$ [ms] and Gaussian noise with mean zero and standard deviation η is added.

Fig. 5 and 6 shows the results for pattern 1 and pattern 2, respectively. Here, $\eta = 0.03$ [p.u.] is used. Each figure shows v_r measured after t_{trig} , v_{rpks} peaks of absolute value of filtered v_r , and the envelope obtained from fitting v_{renv} to the model given in Eqn. (26).

Table 1 and 2 summarize the result of simulations, where for different values of η , the mean and standard deviation of ς and TOF are calculated from 1000 repeated simulated samplings. Tables show that pattern 2 signal produces better result than pattern 1 signal.

If the amplification ratio of received signal and the trigger threshold level are fixed at constant values, since the received signal is attenuated as the measuring distance increases, the number N_{rpks} of peaks that appear before the first envelope peak is decreased. Fig. 5 and 6 shows the results for $N_{rpks} = 10$.

Table 3 and 4 summarize the simulation results for pattern 1 and pattern 2 signals, respectively, where η is kept constant at 0.03 [p.u.] , N_{rpks} is varied from 2 to 10,

Table 1. Simulation result for pattern 1 signal

η[p.u.]	ς_{mean}	$\varsigma_{std}(\times 10^{-6})$	TOF_{mean}[ms]	TOF_{std}[μs]
0.01	0.100	322	2.999	0.260
0.03	0.100	1184	2.999	0.875
0.05	0.099	2258	2.999	1.611

Table 2. Simulation result for pattern 2 signal

η[p.u.]	ς_{mean}	$\varsigma_{std}(\times 10^{-6})$	TOF_{mean}[ms]	TOF_{std}[μs]
0.01	0.100	180	3.000	0.122
0.03	0.100	559	3.000	0.370
0.05	0.100	1021	3.000	0.690

Table 3. Simulation for different N_{rpks} (pattern 1)

N_{rpks}	ς_{mean}	$\varsigma_{std}(\times 10^{-6})$	TOF_{mean}[ms]	TOF_{std}[μs]
2	0.097	5723	2.998	2.522
4	0.098	4405	2.998	2.116
6	0.992	2768	2.999	1.495
8	0.100	1431	2.999	0.976
10	0.100	1184	2.999	0.875

Table 4. Simulation for different N_{rpks} (pattern 2)

N_{rpks}	ς_{mean}	$\varsigma_{std}(\times 10^{-6})$	TOF_{mean}[ms]	TOF_{std}[μs]
2	0.100	570	3.000	0.384
4	0.100	543	3.000	0.363
6	0.100	553	3.000	0.363
8	0.100	559	3.000	0.369
10	0.100	559	3.000	0.370

and the mean and standard deviation of ς and TOF are computed from 1000 repeated simulated samplings. Tables show that pattern 2 signal produces better result than pattern 1 signal.

4. Experimental Results

For the implementation of the proposed method, an experimental setup shown in Fig. 7 is constructed. MPU for the transmitter begins to generate signal patterns right after it sends the synchronization signal ($t = 0$) to the receiver. Receiver MPU stores t_{trig} at the moment when the received signal firstly rises above the threshold voltage, initiates ADC sampling, and continues for some period of time determined by signal pattern. Acquired data is processed by the proposed method to estimate TOF . In the experiment, MA40S4R/S(Murata) is used as ultrasonic transducer. MPUs for the transmitter and receiver are ATmega8535(Atmel) and TMS320F28335(TI), respectively. ADC sampling rate is set to be 2.083[Msps].

The proposed method is fully implemented on TMS320F28335(150 Mhz). The processing time ranges from 6 ms to 8 ms depending on how many peaks are extracted and incorporated into the fitting algorithm,

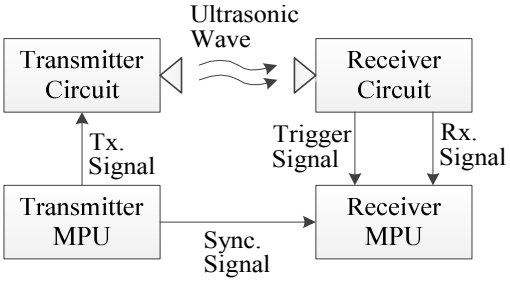

Fig. 7. Experimental setup

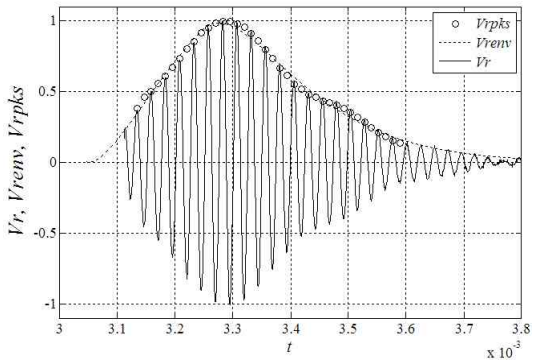

Fig. 8. Experimental result (1m, pattern 1)

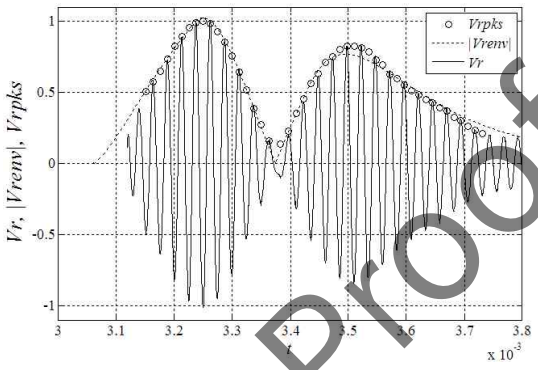

Fig. 9. Experimental result (1m, pattern 2)

implying distance update rate of greater than 100hz is possible. The processing time can be further reduced if σ is fixed at a nominal value of transducer itself obtained by experiments, without being used as one of the fitting parameters as in Step 5.

Fig. 8 and 9 shows the results of 1m distance measurement experimentation for two different signal patterns. Experimentally estimated value of ς of the ultrasonic transducer turns out to be 0.04, implying that the condition given in Eqn. (7) is sufficiently satisfied. Notice that the result of fitting experimental data using approximated envelope model given in Eqn. (26) indicates that the mathematical model for the received signal proposed in this paper is able to closely describe the behavior of actual signals.

Table 5 and 6 summarize the experimental results

Table 5. Experimental result (pattern 1)

Distance [m]	$T_{trig,mean}$[ms]	$T_{trig,std}$ [μs]	TOF_{mean} [ms]	TOF_{std} [μs]
0.5	1.540	6.189	1.487	0.713
1	3.111	7.996	3.044	1.321
1.5	4.542	7.028	4.448	2.724
2	5.989	6.270	5.870	3.477
2.5	7.432	9.425	7.284	4.522
3	8.815	9.817	8.751	5.487

Table 6. Experimental result (pattern 2)

Distance [m]	$T_{trig,mean}$[ms]	$T_{trig,std}$ [μs]	TOF_{mean} [ms]	TOF_{std} [μs]
0.5	1.547	6.528	1.491	0.689
1	3.114	9.206	3.048	0.906
1.5	4.556	6.814	4.449	1.323
2	5.989	5.853	5.859	1.503
2.5	7.427	12.608	7.270	1.808
3	8.821	10.582	8.739	2.102

obtained from 50 repeated measurements at each distance for pattern 1 and pattern 2 signals, respectively. The results verify that the proposed method produces very accurate estimation result for TOF in comparison to conventional window comparator methods and their variations.

Tables show also that the error involved in TOF produced by the proposed method increases as the measuring distance increases. This is mainly because of the fact that as the measuring distance increases, the possibility of original signal pattern being deformed by the reflected wave increases. Despite the fact, Table 5 shows that when signal pattern 2 is used, the standard deviation of TOF is kept less than 2.1 μs if the measuring distance is less than or equal to 3m, which amounts to the distance measurement uncertainty of 0.7 mm. The effect of the reflected wave may be reduced by a weighted least square algorithm having more weight at the leading part of a received signal.

5. Conclusion

This paper derived a mathematical model for the envelope of the received signal assuming damping coefficient involved in the piezoelectric transducers is sufficiently less than 1, as is often the case. This model is used as fitting model in the least square sense for the data obtained through ADC sampling of received signal utilizing two different transmitted signal patterns. The results show that the signal pattern 2 which has two bumps in its envelope performs better in terms of accuracy than the signal pattern 1 which has only one bump in its envelope. When the signal pattern 2 is employed, the uncertainty involved in the estimation of TOF at 1m distance is about 0.9 μs (0.3 mm). Although only two patterns of signals are used in this paper, the

proposed envelope model can be employed in generating diverse signal patterns with more characteristic bumps, which may help to increase the accuracy of *TOF* estimation further.

References

[1] R. Kuc and M.W. Siegel, "Physically Based Simulation Model for Acoustic Sensor Robot Navigation," *IEEE Trans. on Pattern Analysis and Machine Intelligence*, vol. 9, pp. 766-778, Nov. 1987.

[2] H. Peremans, K. Audenaert and J. M. van Campenhout, "A High Resolution Sensor Based on Tri-aural Perception," *IEEE Trans. on Robotics and Automation*, vol. 9, pp. 36-48, Feb. 1993.

[3] J.R. Llata, E.G. Sarabia and J.P. Oria, "Three Dimensional Robot Vision Using Ultrasonic Sensors," *J. Intelligent and Robotic Systems*, vol. 33, pp. 267-284, Mar .2002.

[4] M. Martinez and G. Benet, "Wall-Corner Classification Using Sonar: A New Approach Based on Geometric Features," *Sensors*, pp. 10683-10700, Nov. 2010.

[5] J.C. Jackson, R. Summan, G.I. Dobie, S.M. Whiteley, G. Pierce, and G. Hayward, "Time-of-Flight Measurement Techniques for Airborne Ultrasonic Ranging," *IEEE trans. on Ultrasonics, Ferroelectrics, and Frequency Control.* vol. 60, no. 2, pp. 343-355, Feb. 2013.

[6] E. Kaplan and C. Hegarty, *Understanding GPS: Principles and Applications*, Artech House, 2006.

[7] R. Queiros, R.C. Martins, P.S. Girao, and A. Cruz Serra, "A New Method for High Resolution Ultrasonic Ranging in Air," *proc. of 18th IMEKO World Congress*, Sep. 2006.

[8] R. Queiros, F.C. Alegria, P.S. Girao, and A. Cruz Serra, "Cross-Correlation and Sine-Fitting Techniques for High Resolution Ultrasonic Ranging," *IEEE Trans. on Instrum. and Meas*. vol. 59, no. 12, pp. 3227-3236, May 2010.

[9] J. M. Villadangos, J. Urena, J.J. Garcia, M. Mazo, A. Hernandez, A. Jimenez, D. Ruiz, and C.D. Marziani, "Measuring Time-of-Flight in an Ultrasonic LPS System Using Generalized Cross-Correlation," *Sensors*, vol. 11, pp. 10326-10342, Oct. 2011.

[10] W.G. MaMullan, B.A. Delaughe, and J.S. Bird, "A simple rising edge detector for time of arrival estimation," *IEEE Trans. on Instrum. Meas*. vol. 45, no. 4, pp. 823-827, Aug. 1996.

[11] B. Barshan, "Fast processing techniques for accurate ultrasonic range measurements," *Meas. Sci. Technol.* vol. 11, pp. 45-50. 2000.

[12] E.G. Sarabia, J.R. Llata, S. Robla, C. Torre-Ferrero, and J.P. Oria, "Accurate Estimation of Airborne Ultrasonic Time-of-Flight for Overlapping Echoes," *Sensors*, vol. 13, pp. 15465-15488, 2013.

[13] B. Barshan and R. Kuc, "A Bat-Like Sonar System for Obstacle Localization," *IEEE Trans. on Systems, Man, and Cybernetics,* vol. 22, no. 4, pp. 636-646, July/August 1992.

[14] A. Preumont, *Mechatronics-Dynamics of Electro-mechanical and Piezoelectric Systems*, Springer, 2006.

[15] L.E. Kinsler, A.R. Frey, A.B. Coppens, and J.V. Sanders, *Fundamentals of acoustics*, John Wiley and Sons, 2000.

[16] M. Bartholomew-Biggs, *Nonlinear Optimization with Engineering Applications*, Springer, 2008.

Jin-Hee Choe She received B.S degree in intelligent robot Engineering from Mokwon University, Korea, in 2011. She is currently working toward a Ph.D. degree at Kwangwoon University, Korea. Her research interests include development of ultrasonic devices and their applications.

Kook-Sun Lee He received B.S. degree in Electronics and Communications Engineering, M.S. and Ph.D. degrees in Control and Instrumentation Engineering from Kwangwoon University, Korea, in 2008, 2010 and 2016, respectively. He is currently a post-doctoral researcher in Department of Electrical and Information Engineering, Seoul National University of Science and Technology, Korea. His research interests include nonlinear, robust control for electronic devices and alternative energy systems.

Ick Choy He received B.S., M.S. and Ph.D. degrees in Electrical Engineering from Seoul National University, Korea, in 1979, 1981 and 1990, respectively. From 1981 to 2003, he was with the Intelligent System Control Research Center, Korea Institute of Science and Technology, Korea. He is currently a Professor in School of Robotics, Kwangwoon University, Korea. His research interests include high-performance electrical machine drives, alternative energy systems, and emerging technologies.

Whang Cho He received B.S degree in mechanical engineering from Inha University in 1981 and acquired M.S. and Ph.D. degrees in mechanical engineering from University of Texas at Austin, respectively in 1984 and 1989. He is currently a Professor in School of Robotics, Kwangwoon University in Seoul, Korea. His ongoing researches are focused in development of high precision pose tracking devices, design and control of robotic mobility devices, and development of an energy efficient azimuth thruster system for optimal ship propulsion.